Journal of Solid State Chemistry 182 (2009) 1611–1618

Contents lists available at ScienceDirect

Journal of Solid State Chemistry

journal homepage: www.elsevier.com/locate/jssc

Magnetic and dielectric properties of $YbFe_{2-x}Mn_xO_4$ ($0 \leqslant x \leqslant 1$)

Kenji Yoshii [a,*], Naoshi Ikeda [b], Takamasa Michiuchi [b], Yusuke Yokota [b], Yuka Okajima [a], Yasuhiro Yoneda [a], Yoji Matsuo [c], Yoichi Horibe [d], Shigeo Mori [c,e]

[a] Japan Atomic Energy Agency, Sayo, Hyogo 679-5148, Japan
[b] Department of Physics, Okayama University, Okayama 700-8530, Japan
[c] Department of Physics, Osaka Prefecture University, Osaka 599-8531, Japan
[d] Department of Physics and Astronomy, Rutgers, The State University of New Jersey, New Brunswick, NJ 08854-8019, USA
[e] Department of Materials Science, Osaka Prefecture University, Osaka 599-8531, Japan

ARTICLE INFO

Article history:
Received 30 January 2009
Received in revised form
2 April 2009
Accepted 5 April 2009
Available online 14 April 2009

Keywords:
Multiferroic
Charge ordering
Triangular lattice
Iron oxide
Magnetic properties
Dielectric properties
Electron transfer

ABSTRACT

We have investigated the magnetic and dielectric properties of $YbFe_{2-x}Mn_xO_4$ ($0 \leqslant x \leqslant 1$), which is an Fe-site-substituted system of new multiferroic oxides RFe_2O_4 (R = Y, Ho–Lu). X-ray diffraction measurements show that a solid solution is formed between $YbFe_2O_4$ ($x = 0$) and $YbFeMnO_4$ ($x = 1$) for $0 \leqslant x \leqslant 1$, whereas only compounds with $x = 1$ (i.e., $RM_1M_2O_4$; M_1 and M_2 = trivalent and divalent cations, respectively) have been known for the Fe-site substitution in RFe_2O_4. The valence of the Mn ion is determined to be ~2+, consistently with the suppression of low-temperature magnetization by the Mn substitution. The magnetic transition temperature (T_N) and the dielectric constant (ε') decrease monotonically with increasing x. This result plausibly confirms that the magnetic and dielectric properties in oxides isostructural with RFe_2O_4 are governed by the electron transfer between Fe-site ions, unlike ordinary ferroelectrics and dielectrics, in which the ionic displacement plays a key role. The possibility for application is briefly discussed as well.

1. Introduction

The rare-earth iron oxides RFe_2O_4 (R = Y, Ho–Lu) have a rhombohedral crystal structure (space group $R\bar{3}m$) consisting of an alternating stacking of triangular lattices of R, Fe, and O [1,2]. Recently, we have proposed that this system belongs to a new category of ferroelectrics on the basis of measurements of the resonant X-ray diffraction, electric polarization, and dielectric response: the ferroelectricity below ~330 K is rooted in a polar charge-ordered structure of equimolar Fe^{2+} and Fe^{3+} ions on a triangular lattice [3]. This origin of ferroelectricity is different from that of ordinary ferroelectrics, in which the displacement of cations and anions plays an essential role [4].

In this system, both kinds of Fe ions (Fe^{2+} and Fe^{3+}) have localized magnetic moments. Strong magnetic interactions between these moments lead to ferrimagnetic ordering below T_N~240–250 K [5–9]. Consequently, RFe_2O_4 is regarded as a new kind of multiferroic materials. A correlation between the magnetic and ferroelectric properties is suggested by anomalous electric polarization around ~250 K [3]; such a correlation has been shown by recent experimental and theoretical studies [10,11].

The system is also interesting from the viewpoint of practical applications. The small activation energy required for switching the direction of each polar region (~0.29 eV) offers a possibility for the fabrication of fatigue-free devices [3]. The absence of lead is also suitable for applications because the development of lead-free ferroelectrics is desired to reduce ecological burdens [12].

RFe_2O_4 accommodates the replacement of Fe ions by some other cations, such as Mg^{2+}, Mn^{2+}, Co^{2+}, Cu^{2+}, and Ga^{3+} [13,14]. The replacement leads to isostructural compounds of the form of $RM_1M_2O_4$ ($M_1^{3+} = Fe^{3+}$ and Ga^{3+}; $M_2^{2+} =$ Mg^{2+}, Mn^{2+}, Co^{2+}, Cu^{2+}, and others). Although these materials are assumed to have interesting physical properties, few studies of their properties have been reported [15–18]. Dielectric phenomena, in particular, have not been investigated.

Most recently, we reported the crystallographic, magnetic, and dielectric properties of RFe_2O_4 (R = Tm, Yb, and Lu) and its substituted materials, such as $LuFeCuO_4$ [19–23]. A systematic study showed that the dielectric constant decreased in the order of RFe_2O_4, $RFeCoO_4$, $RFeCuO_4$, and $RGaCuO_4$ (R = Yb and Lu) [21]. The same tendency was also obtained for the isostructural In-substituted system, i.e., $InFe_2O_4$, $InFeCuO_4$, and $InGaCuO_4$ [24]; $InFe_2O_4$ is assumed to show similar charge ordering to that in RFe_2O_4 [25]. The change of the dielectric constant by the Fe-site substitution was interpreted in connection with the inhibition of the electron transfer between the Fe-site ions [21]; the electron

* Corresponding author. Fax: +81 791 58 0311.
E-mail address: yoshiike@spring8.or.jp (K. Yoshii).

0022-4596/$ - see front matter © 2009 Elsevier Inc. All rights reserved.
doi:10.1016/j.jssc.2009.04.008

transfer likely plays a key role in the dielectric response of oxides isostructural with $R\mathrm{Fe_2O_4}$. It was also proposed that these materials may be preferable for applications because of some of their properties, e.g., larger dielectric constants (~2000–6000) as well as lower energy losses than those of $R\mathrm{Fe_2O_4}$ [21,24].

To elucidate more details of the properties of $R\mathrm{Fe_2O_4}$, the aim of the present work is to investigate the synthesis and physical properties of the Mn-substituted system $\mathrm{YbFe_{2-x}Mn_xO_4}$ ($0 \leqslant x \leqslant 1$): we identified the formation of a solid solution for the Mn substitution with $0 \leqslant x \leqslant 1$, while only compounds with equimolar amounts of the trivalent and divalent cations at the Fe site have been reported, as noted earlier, i.e., materials with the formula of $RM_1M_2\mathrm{O_4}$ [13–23]. The magnetic properties of $x = 1$ ($\mathrm{YbFeMnO_4}$) were found to resemble those of the corresponding Y-substituted oxide $\mathrm{YFeMnO_4}$ [16], which shows antiferromagnetic ordering at ~60 K. The magnetic and dielectric measurements for $0 \leqslant x \leqslant 1$ confirm the electron transfer scenario [21,24], together with the valence of Mn ions and the existence of short-range ionic ordering. To make a comparison with the previous data on isostructural materials [20,21,24], the present work deals mainly with the properties below 300 K.

2. Experimental

Polycrystalline samples were prepared by the solid-state reaction [19–24]. The x values of the prepared samples of $\mathrm{YbFe_{2-x}Mn_xO_4}$ were 0, 0.2, 0.4, 0.5, 0.7, 0.8, 0.9, and 1. The reaction was conducted in the flow of a mixed CO–$\mathrm{CO_2}$ gas at 1200 °C for ~72 h. The starting materials were $\mathrm{Yb_2O_3}$, $\mathrm{Fe_2O_3}$, and MnO (Soekawa, 99.9–99.99%). The mixtures of the starting materials were weighted to be ~1.0–1.5 g. The flow ratio of $\mathrm{CO_2}$ against CO ($\mathrm{CO_2}$/CO) was increased from ~2 to ~13 almost linearly with x as x was increased from 0 to 1 in $\mathrm{YbFe_{2-x}Mn_xO_4}$, considering that the Mn substitution increases the Fe valence from 2.5+ ($x = 0$, $\mathrm{YbFe_2O_4}$) to 3+ ($x = 1$ $\mathrm{YbFeMnO_4}$), as assumed from X-ray absorption data discussed later. The sum of the $\mathrm{CO_2}$ and CO flows for each x was commonly ~100 cc/min. During the reaction, the weight loss (~2–3 mg) was in accord with that estimated from the partial reduction of $\mathrm{Fe^{3+}}$ to form the $\mathrm{YbFe_{2-x}Mn_xO_4}$ phase. The oxygen contents, determined by thermogravimetry in a reduced $\mathrm{H_2}$–Ar flow, were ~3.96–3.99(3) and showed no apparent tendency against the Mn content within experimental error.

Powder X-ray diffraction (XRD) measurements using Cu-$K\alpha$ radiation showed the formation of $R\mathrm{Fe_2O_4}$-structure compounds. The XRD patterns were refined by the Rietveld method (RIETAN-2000) [26]. To observe the valence state of Mn ions, X-ray absorption measurements using synchrotron radiation were carried out at the BL14B1 beamline of SPring-8. The photoabsorption of powder samples was measured around the Mn-K edge at room temperature. The magnetic measurements were carried out with a superconducting quantum interference device (SQUID) magnetometer (Quantum Design MPMS). The dielectric properties were measured below 300 K with an impedance analyzer (HP-4284A) equipped with a He refrigerator. Transmission electron microscope (TEM) observations were performed with JEM-2010 at room temperature. The other details have been reported elsewhere [9,19–24].

3. Results

3.1. X-ray diffraction and X-ray absorption

Fig. 1 shows the XRD patterns of $\mathrm{YbFe_{1.6}Mn_{0.4}O_4}$ ($x = 0.4$). The experimental pattern could be refined to the rhombohedral structure of $R\bar{3}m$ assuming a random occupation of the Fe and Mn atoms at the same crystallographic site, as is the case of the isostructural $\mathrm{ErFeMnO_4}$ [27].

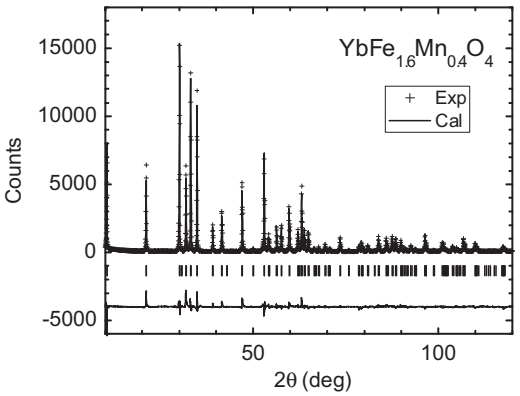

Fig. 1. X-ray diffraction (XRD) patterns of $\mathrm{YbFe_{1.6}Mn_{0.4}O_4}$ ($x = 0.4$, space group $R\bar{3}m$, $R_{WP} = 11.7\%$). The horizontal markers and upper solid line stand for the experimental (Exp) and calculated (Cal) patterns, respectively. The lower solid line shows the difference between the experimental and calculated patterns. The vertical markers are the calculated Bragg angles.

The refinement assuming the same $R\bar{3}m$ structure was also performed for all the other $\mathrm{YbFe_{2-x}Mn_xO_4}$ samples. The lattice parameters are plotted in Fig. 2. The lattice lengths of $\mathrm{YbFe_2O_4}$ ($x = 0$) and $\mathrm{YbFeMnO_4}$ ($x = 1$) were $a = 3.4572(1)$ and $c = 25.1165(7)$ Å for $x = 0$ [21] and $a = 3.4611(1)$ and $c = 25.6515(7)$ Å for $x = 1$, and all of these values are close to those reported previously [13]. For $0 \leqslant x \leqslant 1$, the a-length is almost the same value of ~3.65 Å. On the other hand, with increasing x from 0 to 1, the c-length and the unit-cell volume increased monotonically with increasing x, a result which indicates a formation of solid solutions between $\mathrm{YbFe_2O_4}$ and $\mathrm{YbFeMnO_4}$ for $0 \leqslant x \leqslant 1$. The different x-dependences between the a- and c-lengths are likely associated with the anisotropic stacking structure of this system [1,2] and may affect the magnetic and dielectric properties shown later; however, detailed discussion cannot be made at present.

Fig. 3 shows the X-ray absorption spectra around the Mn-K edge for a representative material ($\mathrm{YbFe_{1.5}Mn_{0.5}O_4}$; $x = 0.5$) and two reference materials (MnO, $\mathrm{Mn^{2+}}$; $\mathrm{Mn_2O_3}$, $\mathrm{Mn^{3+}}$). The subtraction of the background and the normalization of the absorption were made using the IFEFFIT program [28]. The absorption edge of $\mathrm{Mn_2O_3}$ is ~9 eV higher than that of MnO [29]. For $\mathrm{YbFe_{1.5}Mn_{0.5}O_4}$, its absorption edge is located at almost the same photon energy as that of MnO ($\mathrm{Mn^{2+}}$), as pointed by an arrow. Thus, the valence of the Mn ion is ~2+. For $x = 0.4$, 0.7, and 1 as well, we confirmed that their absorption edges were almost identical to that of MnO, strongly suggesting that the valence of the Mn ions is 2+ for $0 \leqslant x \leqslant 1$ in $\mathrm{YbFe_{2-x}Mn_xO_4}$. Accordingly, the $\mathrm{Fe^{2+}}$ ions in $R\mathrm{Fe_2O_4}$ are replaced by $\mathrm{Mn^{2+}}$ in the present series, i.e., the Fe valence changes from 2.5+ to 3+ from $x = 0$ to 1. This result is consistent with that of the isostructural Y-substituted oxide $\mathrm{YFeMnO_4}$ [16]. The valence state of 2+ for the Mn ions explains the suppression of magnetization by the Mn substitution, as discussed later.

3.2. Magnetic properties

Table 1 shows some representative parameters obtained from magnetic measurements discussed in this subsection. The table also provides the result of dielectric measurements noted in the next subsection.

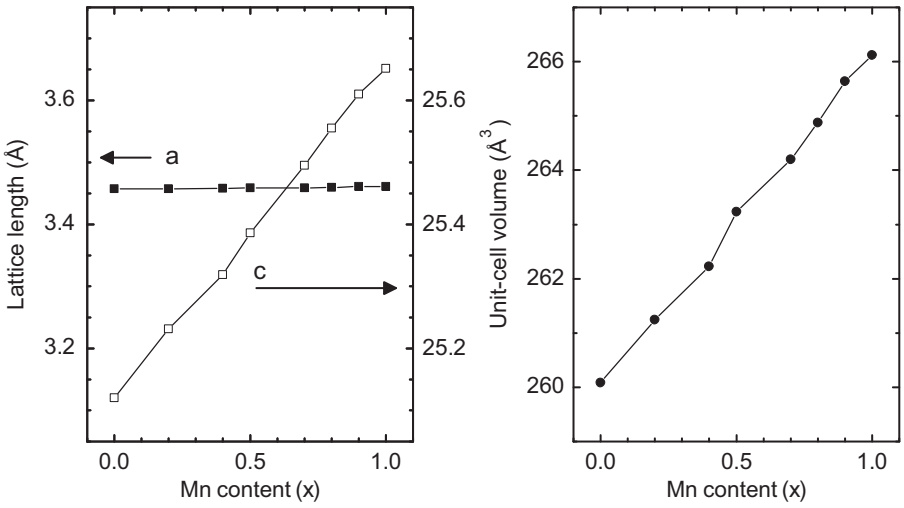

Fig. 2. Lattice lengths and unit-cell volume plotted against x for $YbFe_{2-x}Mn_xO_4$.

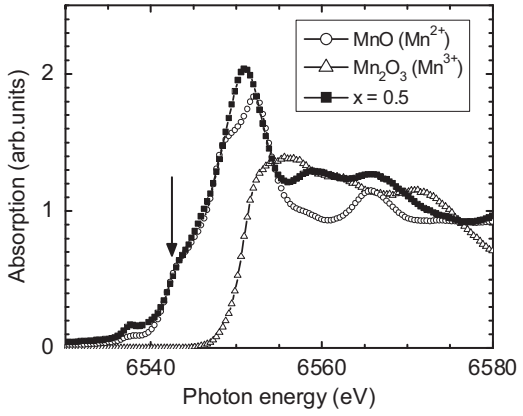

Fig. 3. X-ray absorption spectra at Mn-K edge for $YbFe_{1.5}Mn_{0.5}O_4$ ($x = 0.5$) and reference materials (MnO and Mn_2O_3). The arrow stands for the absorption edge of MnO.

Fig. 4a shows the temperature dependences of the FC (Field-cooled) magnetization (M) for $YbFe_2O_4$ ($x = 0$) taken from Ref. [21]. The upturn of M at 250 K is due to the ferrimagnetic order of Fe^{2+} ($S = 2$) and Fe^{3+} ($S = \frac{5}{2}$) moments. The magnetic transition temperature (T_N) is ~256 K (Table 1), which was determined from the observation of the thermoremanent magnetization (TRM) [21]. A few other characteristics, such as the hump of M at ~130 K, indicate a possible change of the magnetic structure [21].

Fig. 4a also shows the FC and ZFC (zero-field-cooled) magnetization (M) for $YbFe_{1.8}Mn_{0.2}O_4$ ($x = 0.2$), in which 10% of Fe was replaced by Mn. For both the FC and ZFC sequences, M is very smaller than that of $YbFe_2O_4$; M at around 5 K is drastically suppressed down to $\sim\frac{1}{10}$ by the small amount (10%) of the Mn substitution. A peak of the ZFC magnetization is found at ~190 K, below which a deviation of the FC and ZFC curves appears. Below this temperature, we observed the appearance of TRM (inset). Therefore, the inflection at ~190 K is ascribed to ferrimagnetic ordering similar to that in $YbFe_2O_4$ [21]. From the AC susceptibility measurements (see Fig. 5 for brevity), this ordering accompanied by the FC–ZFC deviation may be due to a short-range spin-glass-like phase. The transition temperature will be also denoted as T_N (192 K; Table 1), since antiferromagnetic interactions are dominant from the Curie–Weiss fit, as shown later. The upturn of FC magnetization at low temperatures may be related to either a change of the magnetic structure or a contribution from Yb^{3+} ($4f^{13}$; 4.54 μ_B) [30].

Fig. 4b shows the FC magnetization plotted against the temperature for the representative Mn contents. For each material, a slight inflection is observed at low temperatures, as pointed out for $x = 0.4$ and 1. By observing TRM at low temperatures, it was determined that this inflection is attributed to ferrimagnetic ordering. The transition temperature will be also denoted as T_N because dominant magnetic interactions are antiferromagnetic (see Table 1 and Fig. 4c for brevity). One characteristic feature is that T_N is monotonically lowered from ~256 to ~60 K with increasing x (inset and Table 1). For $x = 1$, its T_N is almost the same as that of $YFeMnO_4$ [16], a reasonable result because of the similar lattice lengths of both oxides [13]. The figure provides another characteristic behavior; the magnetization (M) below T_N is monotonically suppressed with increasing x from 0 to 1. The FC magnetization at 5 K was lowered from ~1200 emu/mol ($x = 0$) to ~100 emu/mol ($x = 1$).

The inverse magnetization for $YbFe_2O_4$ showed a non-Curie–Weiss hyperbolic shape up to 400 K [21]. For $x > 0$, a linear region was observed in the inverse magnetization above ~300 K, as shown for $x = 0.2$ in Fig. 4c. The effective paramagnetic moments (P_{eff}) were smaller (~80–90%) than those calculated by use of Yb^{3+} ($4f^{13}$; 4.54 μ_B) and the spin-only moments of Fe^{3+} ($3d^5$; $S = \frac{5}{2}$; 5.9 μ_B), Fe^{2+} ($3d^6$; $S = 2$; 4.9 μ_B), and Mn^{2+} ($3d^5$; $S = \frac{5}{2}$; 5.9 μ_B). For $YFeMnO_4$, P_{eff} close to the estimated value was obtained for temperatures higher than ~500 K [16]: Magnetic measurements above the highest measurement temperature (400 K) should be made in the future. As the Weiss temperatures (θ) were negative values of ~−150 K, magnetic interactions are antiferromagnetic, similar to those of isostructural oxides such as $YFeMnO_4$ [16,21]. The obtained parameters are listed in Table 1.

Isothermal magnetization at 5 K exhibited a lack of saturated magnetization (not shown), consistent with the ferrimagnetic ordering below T_N. The remanent magnetization was suppressed almost monotonically from ~100 to ~0.1 emu/mol as x was increased from 0 to 1. Accordingly, a ferrimagnetic component was suppressed by the Mn substitution, which is in accord with the suppression of M (Fig. 4).

Fig. 5a shows the real part of the AC magnetic susceptibility (χ') for $YbFe_{1.6}Mn_{0.4}O_4$. A peak at ~160 K, which corresponds to the ferrimagnetic ordering, shifts to higher temperatures with increasing the frequency of the AC magnetic field. The shift width defined as ($\Delta T/T/\Delta \log f$) is ~0.02 (ΔT—peak shift, T—peak temperature and $\Delta \log f$—difference of the logarithm of frequency), which is a typical value for short-range-ordered systems such as spin glasses [31]. The shift width was found to be less than

Table 1
Representative parameters obtained from the magnetic and dielectric measurements of $YbFe_{2-x}Mn_xO_4$.

x	T_N (K) (±2)	P_{eff} (μ_B) (±0.2)	θ (K) (±5)	ε' (RT, 1 kHz) (±100)	α (±0.03)	Q (eV) (±0.03)	ρ (Ω cm; RT)
0	256			12 000	0.08	0.29	$<\sim 1\times10^3$
0.2	192	7.6	−150	9000	0.25	0.25	~ 1–2×10^4
0.4	157	7.4	−140	7500	0.30	0.25	$\sim 5\times10^4$
0.5	135	7.4	−145	6500	0.30	0.25	$\sim 1\times10^5$
0.7	115	7.5	−170	6300	0.20	0.25	~ 3–4×10^5
0.8	92	7.5	−170	6000	0.25	0.25	$\sim 7\times10^5$
0.9	78	7.5	−170	5300	0.27	0.27	$\sim 1\times10^6$
1	62	6.7	−180	5000	0.20	0.30	~ 3–4×10^6

The data of $YbFe_2O_4$ ($x=0$) were taken from Ref. [21]. T_N: magnetic transition temperature (K); P_{eff}: effective paramagnetic moment per formula unit (μ_B); θ: Weiss temperature (K); ε'(RT, 1 kHz): dielectric constant with the applied AC electric field of 1 kHz at room temperature; α: fitting parameter in the Debye model; Q: Activation energy (eV) calculated from tan δ; and ρ: AC resistivity (Ω cm) at around room temperature (RT) obtained from the imaginary part of the dielectric response in the low-frequency region ($\sim<1000$ Hz). See the details in the text.

0.001 for $x=0$, in which the magnetic ordering is of a long-range type [21].

Fig. 5b shows the imaginary part (χ'') for $YbFe_{1.6}Mn_{0.4}O_4$. In the low-frequency region ($<\sim$100 Hz), a broad peak or shoulder was observed below T_N and was found to shift with changing the frequency. The peak could not be detected in the high-frequency data ($>\sim$100 Hz) because of the considerable fluctuation of χ'', for which we have no appropriate explanation. For the low-frequency data ($<\sim$100 Hz) alone, the Arrhenius-type fitting was carried out according to the analysis of $LuFe_2O_4$; $f=f_0\exp(-U/kT)$ (f—AC frequency, f_0—pre-exponential factor, U—activation energy and k—Boltzmann factor) [21,24]. Assuming that the peak in the 10 Hz data is located at the temperature pointed by an arrow, U was calculated to be ∼0.06 eV, which is the energy required for flipping the magnetization of each magnetic cluster [21]. This U value is appreciably smaller than that of the non-Mn-substituted materials ($x=0$), $U\sim$0.30 eV [21].

3.3. Dielectric properties

As reported previously, the end compound $YbFe_2O_4$ ($x=0$) showed large dielectric constants of ∼10 000–20 000 at around room temperature (RT) [21]. Such large dielectric constants are regarded as a characteristic feature of the RFe_2O_4 family [3,9,20,21,32–35].

Large dielectric constants were also obtained for $x>0$. Fig. 6a shows the temperature dependence of the dielectric constant (ε') for another end compound, $YbFeMnO_4$ ($x=1$). The dielectric constants at around RT exhibit fairly large values of ∼5000–10 000, indicating the existence of polar regions and their response against the AC electric field. The data also show that ε' monotonically decreases with increasing the frequency of the AC electric field, a behavior known as dielectric dispersion. This will be discussed later.

Another feature of the dielectric constant is found in Fig. 6b. In other words, the ε' values at around RT (between ∼200 K and RT) decrease with increasing x from 0 to 1. In the present figure, the ε' values were plotted for the AC frequency of 1 kHz alone because ε' was found to somewhat fluctuate for the lower AC frequencies in $YbFe_2O_4$ ($x=0$) [21]. The ε' value at RT decreased from ∼12 000 ($x=0$) [21] down to ∼5000 ($x=1$), as listed in Table 1.

The inset of Fig. 6b shows the AC electrical resistivity (ρ) at around RT for several materials; the values were calculated from the imaginary part (ε'') of the dielectric response [21,36]. All the materials were either semiconducting or insulating below RT, as reported for some isostructural materials [20,21,24]. We also found that the resistivity at around RT increased with increasing x (Table 1); ρ increases from $<\sim$1000 Ω cm ($x=0$) [21] to ∼3–4 × 10^6 Ω cm ($x=1$).

To compare the results with those in previous work, we analyzed the dielectric constant (ε') and tan δ ($\varepsilon''/\varepsilon'$) [20,21,24,32–35]. For the dielectric dispersion (Fig. 6a), the change of ε' against the frequency of the AC field at a certain temperature was fitted with the Debye model (Fig. 7a) [20,21,24,32–35]:

$$\varepsilon' = \varepsilon_1/(1+(i\omega\tau)^{1-\alpha})+\varepsilon_2$$

Here, ω and τ stand for the angular frequency ($\omega=2\pi f$) and the center of the distribution time, respectively. The fitting parameter of α corresponds to the distribution width of the fluctuation time of each polar region [32]. The parameter of α was ∼0.08 for $YbFe_2O_4$ ($<\sim$230 K) [21], almost the same as that of $ErFe_2O_4$ [32,33]. This small value means a narrow distribution width of the fluctuating time, i.e., the dielectric response of the polar regions is coherent [21]. The fitting for $x=0.2$ is shown in Fig. 7a. The analysis was performed at temperatures between ∼150 and ∼250 K, in which a change of ε' was clearly observed in the frequency range of the apparatus (20 Hz–1 MHz). The obtained α of ∼0.25 (Table 1) shows that the coherent response is inhibited by the Mn substitution of 20%. The α values of the other materials were calculated to be ∼0.20–0.30 and exhibited no apparent tendency against x (Table 1).

The tan δ component of $YbFeMnO_4$ ($x=1$) in Fig. 7b exhibits a peak value at a certain temperature, similarly to RFe_2O_4 and some R- and Fe-site-substituted oxides (such as $YbFeCoO_4$) [9,21,35]. The peak temperature and the frequency of the AC field were fitted to the Arrhenius formula, which is essentially identical to that for the AC magnetic susceptibility (Fig. 5)

$$f=f_0\exp(-Q/kT)$$

Here, f and f_0 stand for the AC frequency and the pre-exponential factor, respectively. Q, k, and T mean the activation energy, the Boltzmann constant, and the peak temperature, respectively. The Q value stands for the energy required for switching the direction of each polar region [3,21,32,37]. The obtained Q of $YbFeMnO_4$ was ∼0.30 eV (Table 1). This is close to that of $YbFe_2O_4$, $Q\sim$0.29 eV; this is a typical value of RFe_2O_4 [3,9,21,32,33] and smaller than those of ordinary ferroelectric materials, e.g., $Q\sim$0.9 eV for $Pb(Zr_{0.2}Ti_{0.8})O_3$ (PZT) films [38]. This property plausibly reflects the electronic origin of the dielectric response, i.e., a weak correlation between the dielectric response and the lattice distortion [3]. The Q values for $0<x<1$ were calculated to be ∼0.25–0.27 eV (Table 1), which seem to be slightly smaller than those of $YbFe_2O_4$ ($x=0$) and $YbFeMnO_4$ ($x=1$). However, we consider that these are comparable to the values of $YbFe_2O_4$ and $YbFeMnO_4$ since the errors in the Arrhenius fitting were estimated to be ∼0.03 eV (Table 1). Similar Q values of ∼0.24–0.25 eV were also obtained for the isostructural $HoFe_2O_4$ and Sc-substituted $Lu_{1-x}Sc_xFe_2O_4$ [35].

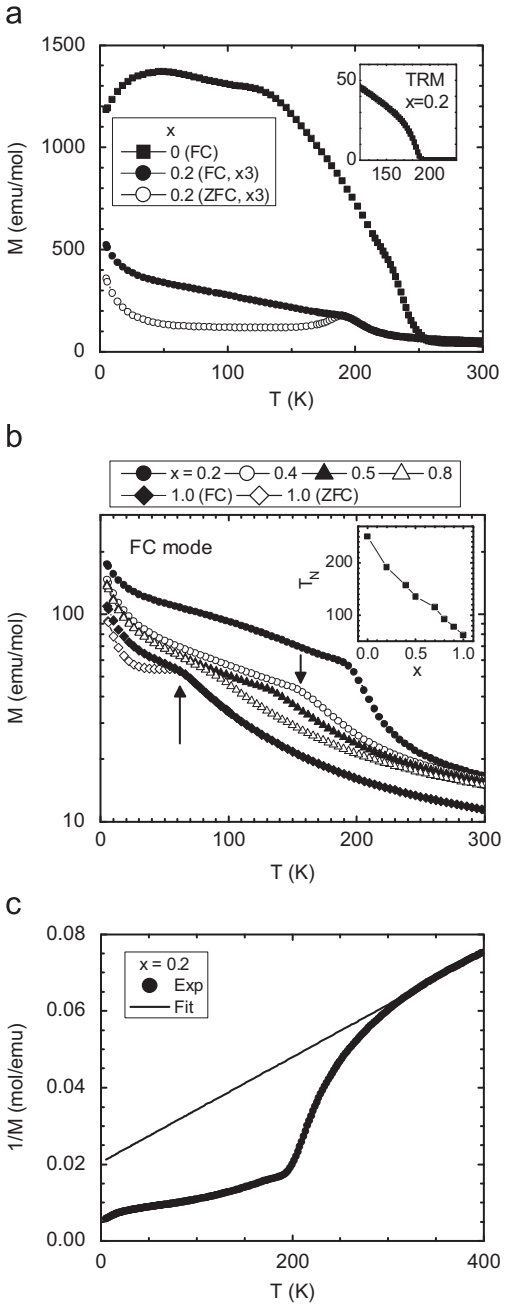

Fig. 4. (a) Magnetization (M) plotted against the temperature (T) for $YbFe_2O_4$ ($x = 0$) and $YbFe_{1.8}Mn_{0.2}O_4$ ($x = 0.2$), measured with the applied magnetic field of 1000 Oe. FC and ZFC stand for field-cooled and zero-field-cooled magnetization, respectively. The magnetization for $x = 0.2$ was multiplied by a factor of 3. The inset shows the thermoremanent magnetization (TRM) for $x = 0.2$. (b) FC magnetization plotted against the temperature for the representative x values in $YbFe_{2-x}Mn_xO_4$. ZFC magnetization was shown only for $x = 1$. The arrow shows the inflection temperatures of the magnetization curve for $x = 0.4$ and 1, close to the magnetic transition temperatures. (c) Inverse magnetization for $x = 0.2$. Exp and fit stand for the experimental data and the Curie–Weiss fitting, respectively.

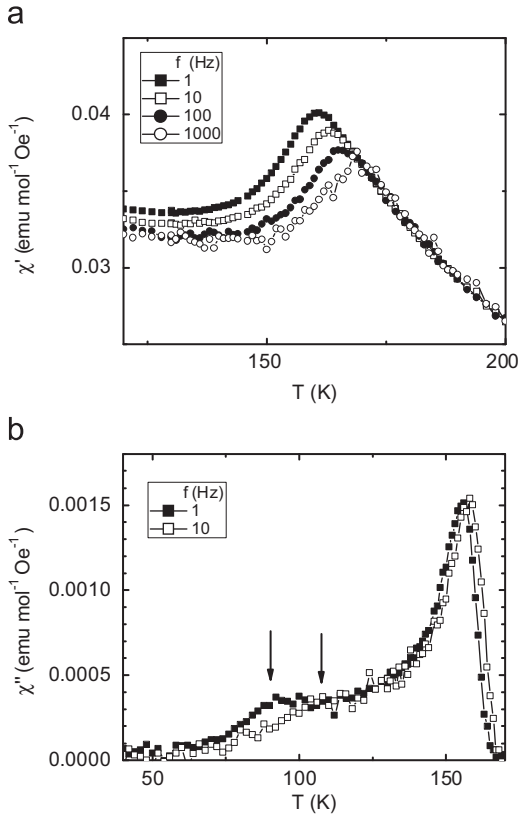

Fig. 5. (a) Real part (χ') of AC susceptibility for $YbFe_{1.6}Mn_{0.4}O_4$ ($x = 0.4$) with the AC frequencies of 1, 10, 100, and 1000 Hz. (b) Imaginary part (χ'') of the AC susceptibility for $x = 0.4$ with the AC frequencies of 1 and 10 Hz. The two arrows indicate the peak temperature or shoulder of χ'' assumed for the Arrhenius fitting.

4. Discussion

4.1. Magnetic properties

The magnetic data provide a few characteristic phenomena of $YbFe_{2-x}Mn_xO_4$. The most characteristic is that the Mn substitution causes the drastic suppression of magnetization (M) and T_N is monotonically lowered to ~60 K with increasing x (Fig. 4b and Table 1). Although the magnetic structures must be determined for a detailed discussion, these phenomena are explained in consideration of the discussion on the isostructural material $LuFeMgO_4$ (Fe^{3+}, Mg^{2+}), in which only Fe^{3+} has a magnetic moment [17].

The replacement of Mn at the Fe site reduces the Fe–Fe magnetic interactions, possibly due to a reduction of the electron transfer at the Fe-ion site [21], plausibly arising from the different energies of Mn- and Fe-3d orbitals. The reduction of the electron transfer is seen from the electrical resistivity (ρ; inset in Fig. 6b and Table 1). The ρ value tends to monotonically increase with increasing x; the electron transfer is suppressed by the energy difference of Fe-3d and Mn-3d electrons [20,21,24]. The decrease in the electron transfer gives rise to a suppression of the magnetic interaction [39], resulting in the lowering of T_N [21]. It is noteworthy that the spin value of the Fe-site ions also governs T_N [21,39]. The spin-only moment of Mn^{2+} is larger ($S = \frac{5}{2}$) than that of Fe^{2+} ($S = 2$), indicating that T_N would increase by the Mn substitution [21,39]. This effect does not explain the experimental result. Therefore, the change of T_N is due to the inhibition of electron transfer. The spin-glass-like behavior (Fig. 5a) is also explained in terms of the magnetic dilution by the Mn substitution, which brings about the shrinkage and distribution of the sizes of magnetic clusters [17,21].

For $YFeMnO_4$, its small magnetization was explained in connection with the absence of an orbital moment in Mn^{2+} ($3d^5$, $S = \frac{5}{2}$) [16]. RFe_2O_4 is regarded as an Ising-like system with magnetic anisotropy [8], which is attributable to the orbital degeneracy of Fe^{2+} ($3d^6$; $S = 2$). This situation manifests itself as the ferrimagnetic component; the direction of the moment is along the c-axis [8]. On the other hand, both the Fe^{3+} ($3d^5$, $S = \frac{5}{2}$) and Mn^{2+} ions in $YFeMnO_4$ have no orbital degeneracy. Thus,

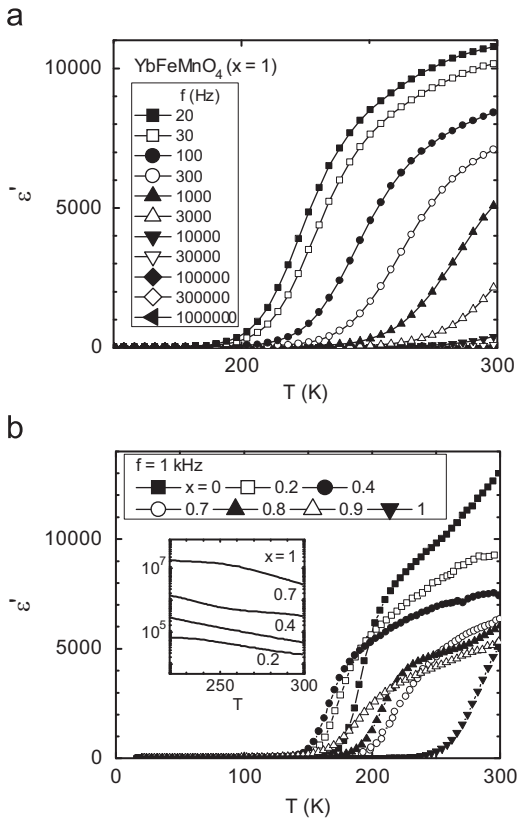

Fig. 6. (a) Dielectric constant (ε') plotted against temperature for $YbFeMnO_4$ ($x = 1$) with the AC frequencies (f) between 20 Hz and 1 MHz. (b) Dielectric constant (ε') for representative x values in $YbFe_{2-x}Mn_xO_4$ with the AC frequency (f) of 1 kHz. The inset shows the AC electrical resistivity at around room temperature (ρ; Ω cm) extracted from the imaginary part (ε'') of the dielectric response.

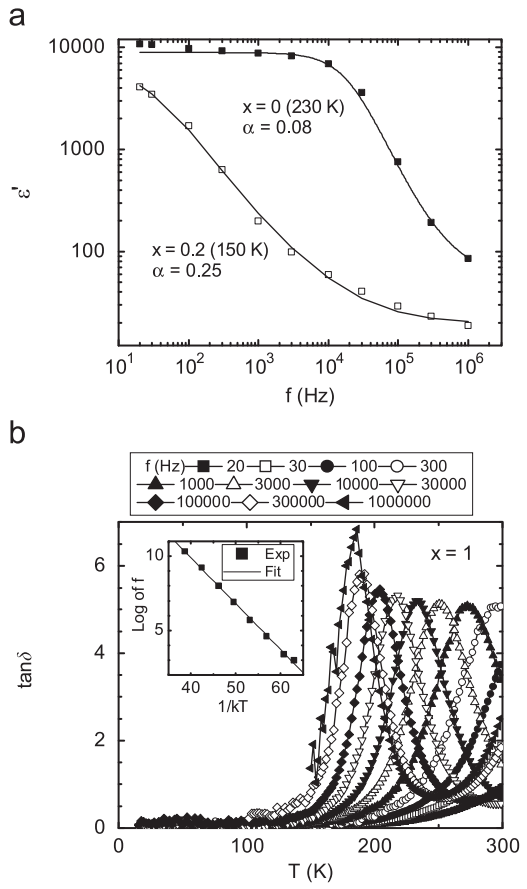

Fig. 7. (a) Dielectric dispersion for $x = 0$ and 0.2 in $YbFe_{2-x}Mn_xO_4$. The values of α are also shown. (b) $\tan\delta$ component plotted against the temperature for $YbFeMnO_4$ ($x = 1$) with the AC frequencies (f) between 20 Hz and 1 MHz. The inset shows the Arrhenius fitting. The ordinate and the abscissa stand for the logarithm of the frequency and the inverse temperature of the peak of $\tan\delta$ ($1/kT$), respectively. The values of kT were expressed in terms of eV.

RFeMnO$_4$ is expressed as an isotropic antiferromagnetic Heisenberg model that exhibits very small remanent magnetization [16]. The monotonic suppression of low-temperature magnetization (M) with increasing x in $YbFe_{2-x}Mn_xO_4$ (Fig. 4b and Table 1) is understood in this context because of the 2+ valence of the Mn ions (Fig. 3).

4.2. Dielectric properties

From the dielectric response (Fig. 6 and Table 1), we concluded that all the materials exhibit fairly large dielectric constants of ~5000–10 000 at around RT for the low AC frequencies. In addition, the activation energies (Q) of $x>0$ (~0.25-0.3 eV) are likely to be comparable to those of $x = 0$ (YFe_2O_4; Q~0.3 eV; Table 1).

For RFe$_2$O$_4$, the large ε' values of ~5000–20 000 and the Q values (~0.3 eV) smaller than those of ordinary ferroelectrics are rooted in the electron exchange between Fe^{2+} and Fe^{3+} (Fig. 8) [3,21,32]. The present results, which are analogous to those of RFe$_2$O$_4$, strongly suggest that the dielectric response in the Mn-substituted materials has the same origin, i.e., the electron transfer between the Fe-site ions, as proposed for some Fe-substituted materials, such as RFeCoO$_4$ (R = Yb and Lu, Q~0.37 eV) [21] and InFeCuO$_4$ (Q~0.29 eV) [24]. We have suggested the importance of the electron transfer in some oxide systems, such as the perovskites La_2RuMO_6 (M = Co and Ni) [40] and $R_{0.5}Ca_{0.5}MnO_3$ (R = Eu–Lu) [41,42].

Regarding Q, we also found that the Q values for $x>0$ (~0.25–0.3 eV) are considerably larger than the activation energies obtained from the magnetic measurements ($U<$~0.1 eV, Fig. 5b). In contrast, both values of RFe$_2$O$_4$ are close to each other ($x = 0$, Q and U of ~0.3 eV) [21], suggesting a correlation of the magnetic and dielectric properties (i.e., multiferroicity). The present result plausibly indicates that multiferroicity is suppressed by the Mn substitution, for which we have no appropriate explanation. However, the different U and Q values for $x>0$ are understood from the discussion in Section 4.1, i.e., the magnetic clusters in $x>0$ materials are rotated more easily than those in RFe$_2$O$_4$ ($x = 0$) owing to the loss of magnetic anisotropy by the Mn^{2+} substitution [16].

The observation of ε' (Fig. 6 and Table 1) means the existence of polar regions for $0\leqslant x\leqslant 1$. For the isostructural LuFeCuO$_4$, electron–diffraction measurements showed the presence of short-range ordering of Fe^{3+} and Cu^{2+} with the $\sqrt{3}\times\sqrt{3}$ structure [19,22], which is accompanied by an electric dipole because the spatial charge distribution is unchanged for the replacement of divalent ions (Cu^{2+} for Fe^{2+}) in the charge-ordered structure in RFe$_2$O$_4$ (Fig. 8) [3,21,24]. Fig. 9a shows the electron diffraction pattern at RT for $YbFe_{1.6}Mn_{0.4}O_4$ ($x = 0.4$), obtained from the transmission electron microscope (TEM) measurement. This pattern for the (hhl) plane (h, l: integers) provides fundamental diffraction spots arising from the $R\bar{3}m$ structure, such as the 110 spot. In addition to these spots, a honeycomb-like pattern, accompanied by diffuse scattering with a weak intensity, is observed, as schematically represented in Fig. 9b. The pattern is nearly identical to that of the isostructural Co-system LuFeCoO$_4$ [23]. Honeycomb-shaped

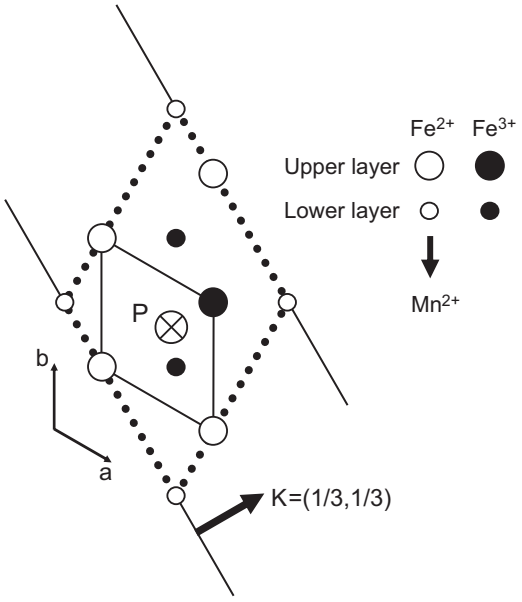

Fig. 8. Charge-ordered $\sqrt{3}\times\sqrt{3}$ structure in the *W*-layer of RFe_2O_4 viewed along the *c*-axis (after Refs. [3,24]). The structure is accompanied by the charge wave shown by vector *K*. The *W*-layer consists of the adjacent upper and lower layers of the Fe ions. The dotted lines show the charge-ordered superlattice, inside which the chemical unit cell is drawn by solid lines. The Fe^{2+} and Fe^{3+} ions are represented by open and filled circles, respectively. Large and small circles stand for the Fe ions in the upper and lower layers, respectively. The 3*d* electrons in the Fe ions are excessive in the upper layer (Fe^{2+}-rich) but deficient in the lower layer (Fe^{3+}-rich); an electric polarization (*P*) appears along the *c*-axis. Vector *P* is directed from the upper to the lower layer. In the Mn substitution, Fe^{2+} is plausibly replaced by Mn^{2+} (see Fig. 9 for more details).

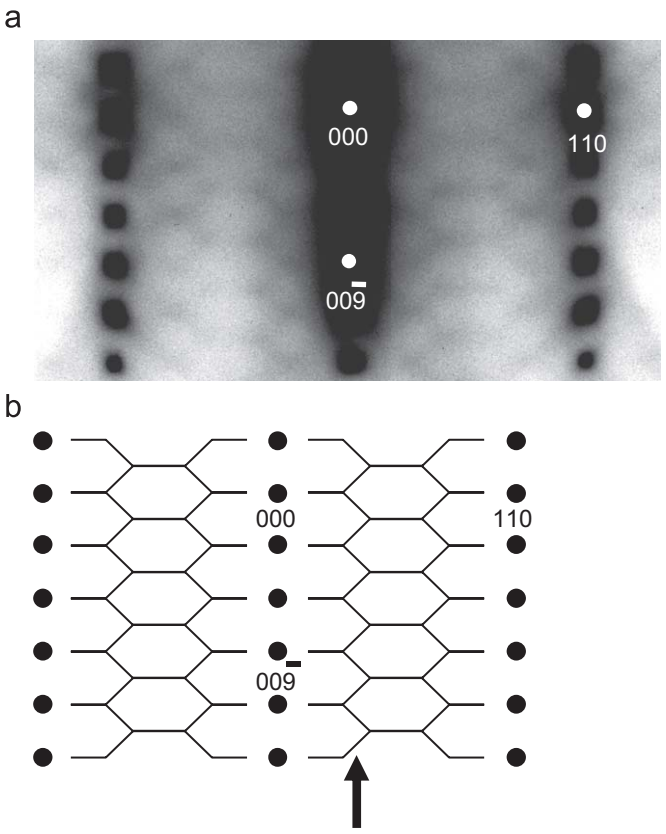

Fig. 9. (a) Electron diffraction pattern of $YbFe_{1.6}Mn_{0.4}O_4$ ($x=0.4$) at room temperature taken along the [1$\bar{1}$0] zone-axis direction. (b) Schematic representation of the scattering pattern seen in (a). The arrow shows honeycomb-shaped diffuse streaks at around the $\frac{1}{3}\frac{1}{3}l$ position (*l*: integer).

diffuse streaks are observed at around the $h/3\,h/3\,l$ positions (h and l: integers), as shown by the arrow for $h=1$ (Fig. 9b). Based on the studies of some binary alloys [43,44], short-range ordering of Fe^{3+} and Co^{2+} ions, similar to that in $LuFeCuO_4$, exists in $LuFeCoO_4$ [23]. Such ordering is plausibly the origin of the dielectric constants of ~1000–2000 at around RT for $LuFeCoO_4$ [21]. From this result, the diffraction pattern (Fig. 9) means that short-range ionic ordering of the trivalent (Fe^{3+}) and divalent (Fe^{2+} and Mn^{2+}) cations exists in the present system (Fig. 8). The diffuse scattering may indicate a spatial fluctuation of the 3*d* electrons in Fe and Mn ions, which shows the importance of electron transfer in the physical properties of RFe_2O_4-structure oxides, consistently with previous studies [21,24] and the discussion presented later. The existence of the short-range ionic ordering also indicates the need for a reinvestigation of the crystal structure of the Fe-site substituted materials.

The value of ε' decreased with increasing x from 0 to 1. This result is interpreted in terms of the inhibition of electron transfer [20,21,24]. Generally, ε' is observed only if polar regions have a response to the AC electric field. As commented earlier, the large ε' of RFe_2O_4 is rooted in the electron transfer between the Fe ions: The electron exchange between Fe^{2+} and Fe^{3+} leads to a reversal of the electric dipole, giving rise to a dielectric response [3,21,32]. The observed ionic ordering (Fig. 9) indicates the occurrence of a similar reversal of the dipole because the dipole is rotated as a result of the 3*d* electron being exchanged between the trivalent (Fe^{3+}) and divalent (Fe^{2+} and Mn^{2+}) cations [21,24]. Considering the increase in resistivity with increasing x (Fig. 6b and Table 1), the electron exchange becomes suppressed for the larger x values, resulting in the lowering of ε' [21]. This discussion is consistent with the results of $InFeCuO_4$ [24] and $YbFeMnO_4$ ($x=1$, Table 1), both of which show a comparable resistivity of $\sim 10^6\,\Omega$ cm and analogous properties, i.e., $T_N=70$ K, $\varepsilon'\sim 6000$ (20 Hz), and $Q\sim 0.29$ eV for $InFeCuO_4$ [24], and $T_N=62$ K, $\varepsilon'\sim 10\,000$ (20 Hz), and $Q\sim 0.30$ eV for $YbFeMnO_4$. The present discussion, together with that in our previous papers [20,21,24], plausibly confirms that the electric dipole in oxides isostructural with RFe_2O_4 is formed by the $\sqrt{3}\times\sqrt{3}$ structure of divalent and trivalent cations (Fig. 8) [19,22] and its response to the AC electric field is governed by the electron transfer between the Fe-site ions, differently from the case of ordinary ferroelectrics and dielectrics, in which the displacement of cations and anions plays a central role.

The larger α values for $x>0$ than that for $x=0$ (Table 1) are in agreement with the lowering of ε' because the lack of coherency (i.e., larger α for $x>0$) suppresses a coherent motion of the polar regions, leading to the lowering of the dielectric constant [21]. The loss of coherency by the Mn substitution is rooted in the shrinkage and spatial distribution of the sizes of the polar regions [21].

Fig. 6b shows that the temperature dependence of ε' is somewhat different for each x, suggesting that the dielectric response is governed by factors other than electron transfer. The ionic ordering of the trivalent (Fe^{3+}) and divalent (Fe^{2+} and Mn^{2+}) cations (Fig. 9) shows that three kinds of polar regions may exist, namely: (1) an Fe^{2+}–Fe^{3+} charge-ordered region, as seen in RFe_2O_4 [3]; (2) a Mn^{2+}–Fe^{3+} region generated by a Mn^{2+} substitution for Fe^{2+} in RFe_2O_4; and (3) an Fe^{2+}/Mn^{2+}–Fe^{3+} region generated by a partial Mn^{2+} substitution for Fe^{2+} in RFe_2O_4. The Mn substitution may induce a complicated change of influential factors on the dielectric response, e.g., the sizes and spatial distributions of the three kinds of polar regions and the Fe/Mn ratio in each polar region. This is supported by the fact that the α value for each material deviated from ~0.2 to ~0.3 and showed no clear tendency against x (Table 1); the spatial coherency between the polar regions is different for each x. This situation may be

associated with the complicated temperature dependence of ε'. A possible defect or excess of oxygen within the experimental errors (Experimental) can have some effects as well [45]. Further investigations should be carried out in order to reveal more details of the dielectric properties of the present system.

A few additional comments should also be made from the viewpoint of application. $YbFeMnO_4$ ($x = 1$) shows the highest resistivity among the present series, i.e., the energy loss caused by the electrical conductivity is the lowest for $x = 1$. Its Q value of ~0.30 eV, comparable to that of RFe_2O_4, indicates a weak correlation between the dielectric response and the lattice distortion [3]. This property offers a possibility for the fabrication of fatigue-free devices using $YbFeMnO_4$ [3]. This property, together with the large ε' of ~5000–10 000 at RT, makes $YbFeMnO_4$ suitable for applications.

In addition, the formation of a solid solution by the Mn substitution encourages further research on RFe_2O_4, considering that elemental substitution has been reported to improve the ferroelectric properties of some materials. For multiferroic $BiFeO_3$, a leakage current was suppressed by 3–5% Mn substitutions, plausibly because of the improvement of the grain structures, which enables the measurement of polarization–electric field (P–E) loops [46]. As the P–E loops of RFe_2O_4 have not been successfully measured thus far, the present result is likely helpful for the measurement. The partial substitution in single-crystalline samples seems to be particularly interesting; in comparison with polycrystals, single crystals are expected to show improvements in their grain structures, as shown in Ref. [46], because they consist of densely packed grains. Such an experiment will be attempted on single-crystalline RFe_2O_4, grown by the floating-zone method [47]. It is also interesting to attempt a synthesis of $RFe_{2-x}M_xO_4$ with M other than Mn from the viewpoints of both fundamental and applied science. The results will be reported in the future.

5. Summary

We have investigated the magnetic and dielectric properties of $YbFe_{2-x}Mn_xO_4$ ($0 \leqslant x \leqslant 1$), which is an Fe-site substituted system of new multiferroic oxides RFe_2O_4 (R = Y, Ho–Lu). X-ray diffraction measurements showed that a solid solution is formed between $YbFe_2O_4$ ($x = 0$) and $YbFeMnO_4$ ($x = 1$) for $0 \leqslant x \leqslant 1$, whereas only compounds with $x = 1$ (i.e., $RM_1M_2O_4$; M_1 and M_2 = trivalent and divalent cations, respectively) have been known for the Fe-site substitution in RFe_2O_4. The valence of the Mn ion was determined to be ~2+, consistently with the suppression of low-temperature magnetization by the Mn substitution. The magnetic transition temperature (T_N) and the dielectric constant (ε') decreased monotonically with increasing x. This result plausibly confirms that the magnetic and dielectric properties in oxides isostructural with RFe_2O_4 are governed by the electron transfer between Fe-site ions, differently from the case of ordinary ferroelectrics and dielectrics, in which the ionic displacement plays a key role. The possibility for application was also briefly commented upon.

Acknowledgments

The authors gratefully thank K. Tokuda and M. Morimoto of Okayama University for their help in dielectric measurements. This work is partially supported by a Grant-in-Aid for Scientific Research (C) from the Ministry of Education, Science, Sports, and Culture.

References

[1] N. Kimizuka, A. Takenaka, Y. Sasada, T. Katsura, Solid State Commun. 15 (1974) 1321.
[2] N. Kimizuka, E. Muromachi, K. Siratori, Handbook on the Physics and Chemistry of Rare Earths, vol. 13, Elsevier Science Press, Amsterdam, 1990, p. 283.
[3] N. Ikeda, H. Ohsumi, K. Ohwada, K. Ishii, T. Inami, Y. Murakami, K. Kakurai, K. Yoshii, S. Mori, Y. Horibe, H. Kito, Nature (London) 436 (2005) 1136.
[4] See for example C. Kittel, Introduction to Solid State Physics, eighth ed., Wiley, New York, 2004.
[5] Y. Nakagawa, M. Inazumi, N. Kimizuka, K. Siratori, J. Phys. Soc. Jpn. 47 (1979) 1369.
[6] M. Kishi, S. Miura, Y. Nakagawa, N. Kimizuka, I. Shindo, K. Siratori, J. Phys. Soc. Jpn. 51 (1982) 2801.
[7] J. Iida, M. Tanaka, H. Kito, J. Akimitsu, J. Phys. Soc. Jpn. 59 (1990) 4190.
[8] J. Iida, M. Tanaka, Y. Nakagawa, S. Funahashi, N. Kimizuka, S. Takekawa, J. Phys. Soc. Jpn. 62 (1993) 1723.
[9] K. Yoshii, N. Ikeda, A. Nakamura, Physica B 378–380 (2006) 585.
[10] M.A. Subramanian, T. He, J. Chen, N. Rogado, T.G. Calvarese, A.W. Sleight, Adv. Mater. (Weinheim Ger.) 18 (2006) 1737.
[11] M. Naka, A. Nagano, S. Ishihara, Phys. Rev. B 77 (2008) 224441.
[12] See, for example, J. Ryu, J.-J. Choi, B.-D. Hahn, D.-S. Park, W.-H. Yoon, K.-H. Kim, Appl. Phys. Lett. 90 (2007) 152901.
[13] N. Kimizuka, E. Takayama, J. Solid State Chem. 40 (1981) 109.
[14] N. Kimizuka, E. Takayama, J. Solid State Chem. 41 (1982) 166.
[15] Y. Todate, E. Himoto, C. Kikuta, M. Tanaka, J. Suzuki, Phys. Rev. B 57 (1998) 485.
[16] J. Iida, M. Tanaka, Y. Nakagawa, J. Phys. Soc. Jpn. 59 (1990) 4443.
[17] N. Ikeda, K. Kohn, E. Himoto, M. Tanaka, J. Phys. Soc. Jpn. 64 (1990) 4371.
[18] T. Sunaga, M. Tanaka, N. Sakai, Y. Tsunoda, J. Phys. Soc. Jpn. 70 (2001) 3713.
[19] Y. Matsuo, Y. Horibe, S. Mori, K. Yoshii, N. Ikeda, J. Magn. Magn. Mater. 310 (2007) 349(E).
[20] K. Yoshii, N. Ikeda, S. Mori, J. Magn. Magn. Mater. 310 (2007) 1154.
[21] K. Yoshii, N. Ikeda, Y. Matsuo, Y. Horibe, S. Mori, Phys. Rev. B 76 (2007) 024423.
[22] Y. Matsuo, M. Suzuki, Y. Noguchi, T. Yoshimura, N. Fujimura, K. Yoshii, N. Ikeda, S. Mori, Jpn. J. Appl. Phys. 47 (2008) 8464.
[23] Y. Matsuo, A. Hirata, Y. Horibe, K. Yoshii, N. Ikeda, S. Mori, Ferroelectrics (2009) in press.
[24] K. Yoshii, N. Ikeda, Y. Okajima, Y. Yoneda, Y. Matsuo, Y. Horibe, S. Mori, Inorg. Chem. 47 (2008) 6493.
[25] K. Oka, M. Azuma, N. Hayashi, S. Muranaka, Y. Narumi, K. Kindo, S. Ayukawa, M. Kato, Y. Koike, Y. Shimakawa, M. Takano, J. Phys. Soc. Jpn. 77 (2008) 064803.
[26] F. Izumi, T. Ikeda, Mater. Sci. Forum 321–324 (2000) 198.
[27] M. Nespolo, M. Isobe, J. Iida, N. Kimizuka, J. Alloys Compd. 313 (2000) 59.
[28] B. Ravel, M. Newville, J. Synchrotron Radiat. 12 (2004) 537.
[29] G. Subías, J. García, M.G. Proietti, J. Blasco, Phys. Rev. B 56 (1997) 8183.
[30] J.H. Van Vleck, The Theory of Electric and Magnetic Susceptibilities, Oxford University Press, Oxford, 1965.
[31] J.A. Mydosh, Spin Glasses, Taylor and Francis, London, 1993.
[32] N. Ikeda, K. Kohn, H. Kito, J. Akimitsu, K. Siratori, J. Phys. Soc. Jpn. 63 (1994) 4556.
[33] N. Ikeda, K. Kohn, H. Kito, J. Akimitsu, K. Siratori, J. Phys. Soc. Jpn. 64 (1995) 1371.
[34] N. Ikeda, K. Kohn, N. Myouga, E. Takahashi, H. Kitoh, S. Takekawa, J. Phys. Soc. Jpn. 69 (2000) 1526.
[35] K. Yoshii, Y. Yoneda, D. Maeda, Y. Yokota, T. Michiuchi, T. Komatsu, N. Ikeda, Y. Matsuo, S. Mori, Jpn. J. Appl. Phys. 47 (2008) 7599.
[36] G.P. Mazzara, S. Skirius, G. Cao, G. Chern, R.J. Clark, J.E. Crow, H. Mathias, J.W. O'Reilly, L.R. Testardi, Phys. Rev. B 47 (1993) 8119.
[37] D. Zipse, N.S. Dalal, R. Vasic, J.S. Brooks, P. Kögerler, Phys. Rev. B 71 (2005) 064417.
[38] C.S. Ganpule, A.L. Roytburd, V. Nagarajan, B.K. Hill, S.B. Ogale, E.D. Williams, R. Ramesh, J.F. Scott, Phys. Rev. B 65 (2001) 014101.
[39] See, for example, K. Yosida, Theory of Magnetism, Springer, New York, 1996.
[40] K. Yoshii, N. Ikeda, M. Mizumaki, Phys. Stat. Sol. A 203 (2006) 2812.
[41] Y. Hiramitsu, K. Yoshii, Y. Yoneda, J. Mizuki, A. Nakamura, Y. Shimojo, Y. Ishii, Y. Morii, N. Ikeda, Jpn. J. Appl. Phys. 46 (2007) 7171.
[42] K. Yoshii, Y. Hiramitsu, Y. Yoneda, Y. Okajima, Y. Nishihata, J. Mizuki, N. Ikeda, Ferroelectrics (2009) in press.
[43] R. De Ridder, G. Van Tendeloo, S. Amelinckx, Acta Cryst. A 32 (1976) 216.
[44] R. De Ridder, G. Van Tendeloo, D. Van Dyck, S. Amelinckx, Phys. Stat. Sol. A 38 (1976) 663.
[45] S. Mori, S. Shinohara, Y. Matsuo, Y. Horibe, K. Yoshii, N. Ikeda, Jpn. J. Appl. Phys. 47 (2008) 7595.
[46] S.K. Singh, H. Ishiwara, K. Maruyama, Appl. Phys. Lett. 88 (2006) 262908.
[47] T. Michiuchi, Y. Yokota, T. Komatsu, H. Hayakawa, D. Maeda, T. Kuroda, N. Hanasaki, T. Kambe, Y. Matsuo, S. Mori, K. Yoshii, N. Ikeda, Ferroelectrics (2009) in press.